

Interplay of hydrogen bonding and molecule-substrate interaction in self-assembled adlayer structures of a hydroxyphenyl-substituted porphyrin

Lars Smykalla^a, Pavel Shukrynau^a, Carola Mende^b, Tobias Rüffer^b, Heinrich Lang^b,
Michael Hietschold^a

^a*Technische Universität Chemnitz, Institute of Physics, Solid Surfaces Analysis Group, D-09107 Chemnitz, Germany*

^b*Technische Universität Chemnitz, Institute of Chemistry, Inorganic Chemistry, D-09107 Chemnitz, Germany*

Abstract

The formation of hydrogen-bonded organic nano-structures and the role of the substrate lattice thereby were investigated by scanning tunneling microscopy. The self-organization of 5,10,15,20-tetra(*p*-hydroxyphenyl)porphyrin (H₂THPP) molecules leads to two molecular arrangements on Au(111). One of these is characterized by pair-wise hydrogen bonding between hydroxyl groups and a low packing density which enables a rotation of individual molecules in the structure. A different interaction with stronger chain-like hydrogen bonding and additional interactions of phenyl groups was observed for the second structure. The influence of the substrate on the epitaxial behavior is demonstrated by the adsorption of H₂THPP on the highly anisotropic Ag(110) substrate. There, several balances between the occupation of favorable adsorption positions and the number of hydrogen bonds per molecule were found. The molecules form molecular chains on Ag(110) and also assemble into two-dimensional periodic arrangements of differently sized close-packed blocks similar to the second type of supramolecular ordering found on Au(111). Dispersion corrected Density Functional Theory calculations were applied to understand the adsorption and complex epitaxy of these molecules. It is shown that the azimuthal orientation of the saddle-shape deformed molecule plays an important role not only for the intermolecular but also for the molecule-substrate interaction.

1. Introduction

The bottom-up fabrication of molecular nano-devices with advanced functions is a subject of significant interest.^{1–3} The construction of desired molecular network architectures on suitable substrates is achieved by the self-assembly of molecular building blocks, which is mainly controlled by a complex interplay between non-covalent bonds such as hydrogen bonds, van der Waals and electrostatic interactions, and the epitaxy on the substrate.^{4–14} From the knowledge gained about the delicate balance between intermolecular and molecule-substrate interactions, the functional nano-networks can then be tuned by adjusting functional groups of the molecule to gain the desired architectures^{15–17} and the interface electronic structure for the specific application. Therefore, it is important that the molecular orientation, configuration and conformation, and the interactions between the adsorbed molecules and the substrate as well as between molecules can be identified and understood, e.g. by using scanning tunneling microscopy (STM).

Porphyrins and their appropriate metal complexes are a very important class of molecules, which are responsible for the functionality in many biological systems. The stability and exceptional versatility of porphyrins led to great interest in the self-assembly of these molecules on surfaces for nano-technology.¹⁸ Numerous studies demonstrate that porphyrin-based molecules tend to arrange themselves in well-defined long-range ordered lateral structures.^{19–23} The combination of both functionality and structure makes them ideal candidates for molecular devices with

applications, such as for electronics, spintronics²⁴, data storage²⁵, non-linear optics²⁶, sensors²⁷, solar cells²⁸, catalysts²⁹, as well as for tumor photosensitizers and photodynamic therapy^{30–32}. In this study, we use hydroxyphenyl functional groups at the meso positions of a porphyrin molecule to enhance the intermolecular interaction and self-assembly properties *via* hydrogen bonding^{33–37}.

For hydrogen-bonded networks, often an incommensurate registry between the lattices of the close-packed molecular layer and the substrate can be expected. Weak intermolecular interactions and large energetic differences in adsorption sites likely result in a commensurate epitaxy or coincidence with a commensurate super cell.³⁸ On the other hand, the prediction of the specific mode represents a problem if the molecular arrangement is determined by strong intermolecular interactions but also the substrate plays a major role in the epitaxy. The mechanisms by which the molecular self-assemblies compensate for the incommensurateness of the lattice parameters of their close-packed crystal structures are then of particular interest. Au(111) was chosen as a surface with a flat and Ag(110) as one with an highly anisotropic and corrugated surface potential. Results for the novel molecular structures formed on these substrates and the investigation of the interactions involved in the self-organization of the molecules are presented in the following.

2. Methods

2.1. Experimental details

5,10,15,20-tetra(*p*-hydroxyphenyl)porphyrin (H₂THPP) was synthesized analogous to a published procedure.^{25,39} Clean surfaces of the Au(111) and Ag(110) single crystals were prepared by multiple cycles of Ar⁺ sputtering at an energy of 500 eV and annealing to 400 °C for 1 h. H₂THPP molecules were deposited on the substrate by organic molecular beam epitaxy in ultra high vacuum (UHV). For this, solid H₂THPP was first purified by heating to a temperature slightly below the sublimation temperature in UHV. The molecules were then deposited at around 350 °C on the clean Au(111) and Ag(110) surfaces. The temperature of the substrate during deposition was kept at room temperature. The scanning tunneling microscopy experiments were performed with a variable-temperature STM from Omicron in UHV. The base pressure in the UHV chamber was in the range of 10^{−10} mbar. Electrochemically etched tungsten tips were used for the STM. All measurements were done at room temperature (ca. 23 °C). STM images were measured in constant current mode with a tunneling current of 100 pA. The bias voltage as referred to in the figure caption was applied to the sample. STM data was processed with the WSxM software⁴⁰ whereby moderate low-pass filtering was used for reduction of noise.

2.2. Computational details

Density Functional Theory (DFT) calculations were performed with the grid-based projector augmented wave method (GPAW)⁴¹. The revised version of the exchange-correlation functional of Perdew, Burke and Ernzerhof (RPBE)⁴² was used in the calculations for different adsorption sites and energy barriers for diffusion and rotation. For the dispersive interactions not accounted for in DFT⁴³, the correction from Tkatchenko and Scheffler⁴⁴ (vdW(TS)) was added, which is known to give good adsorption distances and energies at very low additional computational cost.⁴⁵ The proposed vdW-parameters by Ruiz *et al.*⁴⁶ were used, which include screening effects of the metal surfaces. We applied the LCAO mode⁴⁷ of GPAW, where the pseudo density is evaluated on a fine grid, whereas a double- ζ plus valence polarization type basis set is used for the wave functions. A slab of 5 Ag layers with periodic boundary conditions in the x and y directions was used to model the Ag(110) substrate. In the same way the Au(111) surface is modeled by a 5 layer thick slab of Au atoms. Due to its large periodicity, the reconstruction of the Au(111) surface is not considered within our calculations. A lattice constant of 4.09 Å for Ag and 4.17 Å for Au was used and 7 Å wide vacuum was added in z direction on each side of the substrate slab with the adsorbed molecule. For the Brillouin zone sampling, only the Γ -point was deemed

to be sufficient because of the large size of the cell. The topmost substrate layer and all atoms of the molecule were allowed to relax during optimization. Adsorption energies were calculated by subtracting the total energy of the individual molecule and substrate from the total energy of the combined molecule-substrate system: $E_{\text{ad}} = E_{\text{mol+subst}} - E_{\text{mol}} - E_{\text{subst}}$.

3. Results and Discussion

3.1. Adlayer structures of H_2THPP on $\text{Au}(111)$

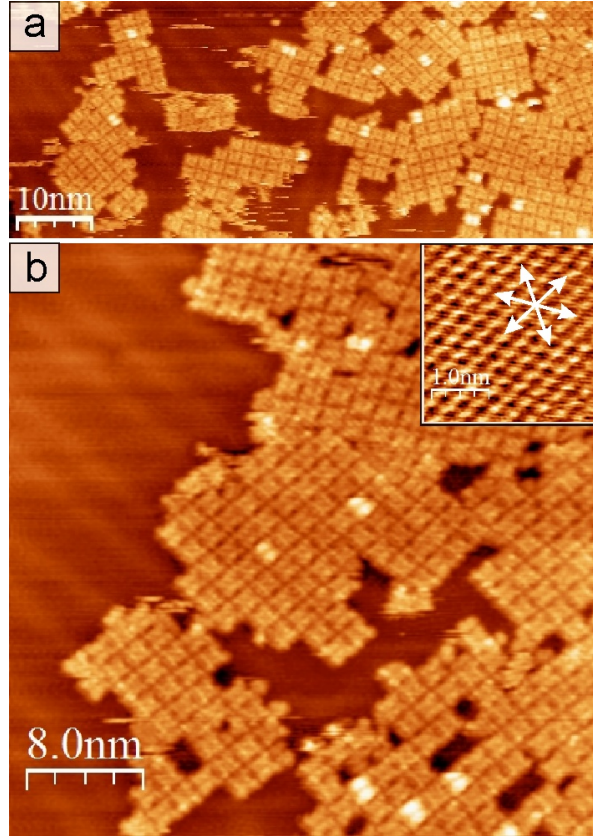


Figure 1: (a),(b) Formation of small islands at submonolayer coverage. Molecules on top of the first layer appear brighter. Inset in (b): atomically resolved Au lattice. Arrows are along the direction of the unit cell vectors of the $\text{Au}(111)$ substrate.

Upon adsorption of H_2THPP molecules on the $\text{Au}(111)$ surface, the molecules begin to arrange in small islands. As can be seen in Fig. 1, at a coverage of around 0.8 of a molecular monolayer, these islands have a structure with a square molecular unit cell and domains which are rotated by 120° with respect to each other due to the threefold symmetry of the $\text{Au}(111)$ surface. The domain walls (pairs of corrugation lines) from the $22 \times \sqrt{3}$ reconstruction of $\text{Au}(111)$ are visible in the left part of Fig. 1(b). The reconstruction is visible through the first monolayer (Fig. 2), which is an indication for a weak molecule-substrate interaction (physisorbed molecules). At room temperature, the molecules are mobile on the surface (small stripes from movement while scanning in Fig. 1(a)) and the rearrangement and growth of the small domains can be followed with STM. Furthermore, a few individual H_2THPP molecules adsorbed on top of an underlying molecule (Fig. 1(a)). After the sample was annealed at around 150°C , very large highly ordered areas of one domain are found (Fig. 2). Monolayer islands of this structure expand continuously over step edges of the $\text{Au}(111)$ substrate with the centers of the tilted H_2THPP molecules located directly over the step edge (right inset of Fig. 2). One unit cell vector of the molecular structure

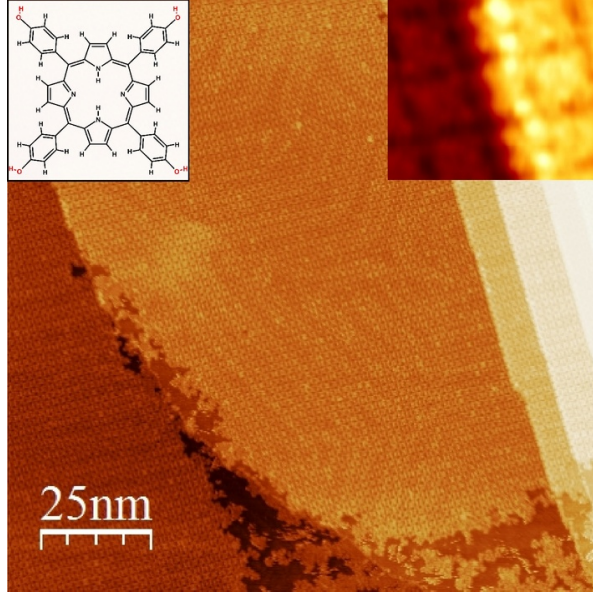


Figure 2: Large ordered monolayer of H₂THPP on Au(111) after annealing to ≈ 150 °C. Inset left: chemical structure of H₂THPP; inset right: zoom on molecules adsorbed on a step edge of the Au substrate.

is parallel to one lattice vector of Au(111). A highly resolved STM image of the square molecular arrangement is displayed in Fig. 3. The lattice parameters measured with STM for the square structure are $|\vec{A}| = (1.74 \pm 0.04)$ nm, $|\vec{B}| = (1.64 \pm 0.04)$ nm and the angle between both unit cell vectors is $\alpha = (87 \pm 1)^\circ$. In the error margin of the measured values a point-on-line epitaxy³⁸ can be found, where H₂THPP adsorbs commensurately on identical adsorption positions along $\vec{A} = 6 \cdot \vec{a} \approx 1.732$ nm (Fig. 3(c)). In this rectangular arrangement, hydroxyl groups of adjacent molecules form O-H \cdots O hydrogen bonding pairs.

The appearance of the molecules is different for positive (empty states, Fig. 3(a)) and negative bias voltage (filled states, Fig. 3(a)), respectively. The general shape of the H₂THPP molecule with the four tilted phenyl groups and the depression in the center is seen at negative bias voltage. At positive voltage, H₂THPP was imaged as two pairs of protrusions which originate from π electrons of the pyrrolic carbon atoms on a saddle-shaped porphyrin macrocycle. It is known that 5,10,15,20-tetraphenylporphyrin (TPP) molecules adsorbed on a metal surface show a non-planar deformation of the central porphyrin unit.^{21,36,48} It is characterized by the bending of pairs of opposite pyrrole rings above and below the porphyrin mean plane, respectively, to form a saddle-shape. This conformation is induced by the steric repulsion from the phenyl rings, which are rotated toward a more parallel adsorption geometry to increase the interaction of the π electrons with the surface. A mirror plane defined by the molecular saddle-shape is rotated by $\delta_B = (4 \pm 2)^\circ$ relative to \vec{B} . Within the molecular layer and also on top of step edges of Au(111) individual molecules can be rotated randomly by 90° . This is possible because in this structure the intermolecular interaction is dominated by weak hydrogen bonding and does not include a more rigid π - π stacking of phenyl groups⁴⁹ as in the case of metal- and free-base TPP molecules on (111) metal surfaces^{19,21,23}, where all molecules have a fixed orientation. An azimuthal 90° rotation of individual H₂THPP molecules in the molecular network can be occasionally induced by the tip while scanning, which is demonstrated in Fig. 3(d). If the two successively measured images are compared with each other, correspondingly rotated molecules can be identified (marked with squares). This change is indeed a rotation of the full molecule in the structure and not a flipping of the saddle-shape deformation as evidenced by the rotation of a defective molecule with one missing phenyl group, which is marked with a circle in Fig. 3(d). This indicates a higher degree of freedom for the individual molecules in the structure which is stabilized by

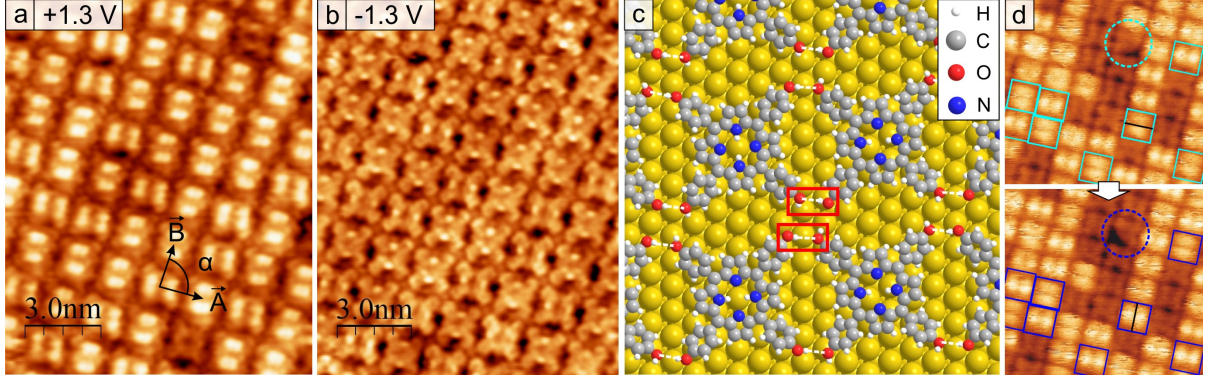


Figure 3: Highly resolved filled (a) and empty molecular states (b) STM image of the square structure of H_2THPP on $\text{Au}(111)$. (c) Model for the arrangement of H_2THPP molecules in this structure. Pair-wise hydrogen bonding is marked with red rectangles. (d) Molecules which are rotated by 90° in the subsequently measured image (bottom) are marked by squares. A rotated molecule with one missing phenyl group is indicated by a dotted circle ($11.0 \text{ nm} \times 10.5 \text{ nm}$, $U = +1.2 \text{ V}$).

weak hydrogen bonds between hydroxyl groups compared the pattern with π - π -stacking. The two different appearances of this molecule at higher bias voltages, which become evident from Fig. 3(d), and the correlated electronic structure are discussed elsewhere.²⁵

At submonolayer coverages only the square structure was found. A second type of arrangement of H_2THPP molecules was observed on the $\text{Au}(111)$ surface together with the aforementioned structure for coverages close to one complete monolayer. The unit cell is oblique with an angle of $\beta = (70 \pm 2)^\circ$ (Fig. 4). The packing density of this array is (0.42 ± 0.04) molecules per nm^2 and clearly larger than that of the square structure with (0.35 ± 0.02) molecules per nm^2 . The epitaxial angle of the adsorbate lattice with respect to the $\text{Au}(111)$ lattice is around 20° , which was measured by using the corrugation lines of the Au reconstruction. The marked area in Fig. 4(a) is a lattice defect in the form of a small domain of the square structure, which demonstrates that one lattice vector of both structures is identical. Fig. 4(b) shows the oblique structure at higher bias voltage where the saddle-shape of individual molecules can be seen. All molecules along one lattice vector (dotted lines) have an identical orientation of the saddle-shaped macrocycle ($(24 \pm 4)^\circ$ relative to this vector), whereas along the other lattice vector the molecules are rotated alternately by circa 90° . Molecules in every second row appear less resolved in Fig. 4(b) due to the orientation of the saddle-shape nearly vertical to the fast scanning direction (clearly resolved two protrusions if the scanning direction is rotated by 90°). The model for the structure and its coincident epitaxy on $\text{Au}(111)$ is presented in Fig. 4(c). For the molecular arrangement in the unit cell with an angle of 70° , hydrogen bonding is always zigzag-chain-wise between four hydroxyl groups. Compared to the square structure, this increases the number of hydrogen bonds per molecule from two to three and, thus also, the overall intermolecular interaction. A similar triple hydrogen bonding scheme was reported before for 5,10,15,20-tetrakis(3,5-dimethyl-4-hydroxyphenyl)porphyrin on $\text{Cu}(111)$.³⁶ Moreover, for the crystal structure of this molecule Hill *et al.*³⁶ found arrays of hydrogen-bonded molecules, whose bonding scheme resembles that of the square structure in our system. In the oblique arrangement of H_2THPP , the planes of the phenyl groups are always parallel to each other (black, dotted rectangle in Fig. 4(c)). We propose that a vertical arrangement of the hydroxyphenyl groups would lead to steric hindrance and a parallel-displaced π - π interaction is more favorable^{49,50}. Thus, this leads to the row-wise and rigid azimuthal 90° alternation of the saddle-shaped H_2THPP molecules. A clearly defined fixed orientation was also observed for TPP with an identical rotation of all molecules within the molecular structure, which was explained by the “T-stacking” of the phenyl rings.^{21,23}

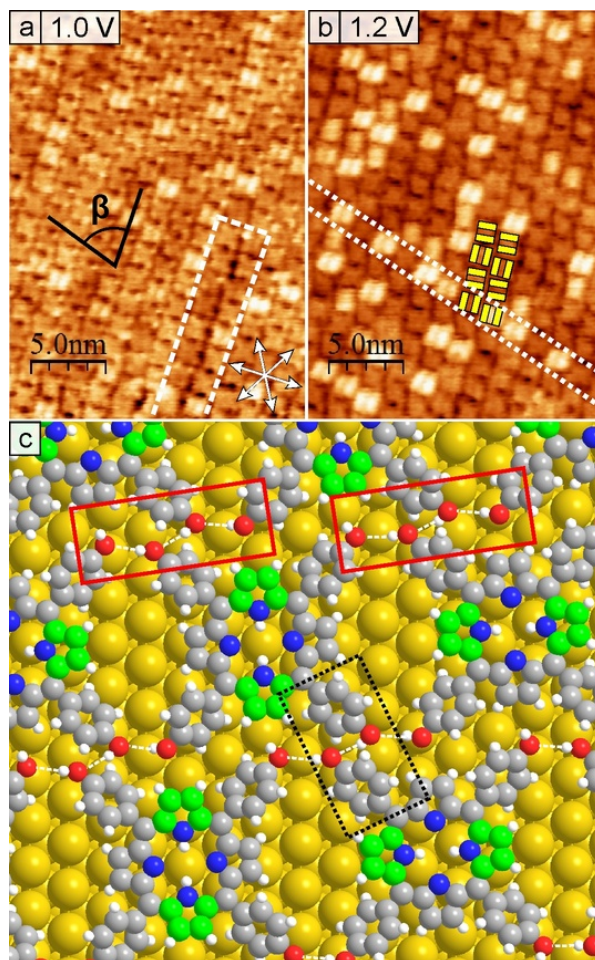


Figure 4: STM images of the oblique structure of H_2THPP on $\text{Au}(111)$: (a) The Au reconstruction lines are weakly visible through the molecular monolayer. A lattice defect by the square arrangement is marked. (b) At higher bias voltage the saddle-shape of H_2THPP (indicated by yellow rectangles) can be identified - along the direction of one lattice vector molecules have identical and along the other vector alternating orientations. (c) Model of the molecular arrangement. The interaction of the phenyl groups is marked exemplarily in black, hydrogen bonding in red and the protruding C atoms of the saddle-shaped molecule in green.

3.2. Adlayer structures of H_2THPP on $\text{Ag}(110)$

To acquire knowledge about the influence of the corrugation of the surface potential on the epitaxy and supramolecular ordering, the adsorption of H_2THPP on the highly anisotropic $\text{Ag}(110)$ substrate was also investigated. Immediately after deposition of a submonolayer coverage, most molecules on the surface were disordered (not shown) and single molecules could be stably imaged at room temperature, which indicates a lower diffusion activity of H_2THPP molecules on $\text{Ag}(110)$ than on $\text{Au}(111)$. Post-annealing of the sample to $150\text{ }^\circ\text{C}$ increased the mobility, resulting in the formation of many small ordered islands on the substrate terraces (Fig. 5(b)). A typical molecular island consisted of nine or twelve molecules. During heating to circa $200\text{ }^\circ\text{C}$ the molecules rapidly diffused and rearranged into molecular chains, striped islands and differently ordered areas, which are shown in Fig. 5(a).

Each structure can occur mirrored relative to the $[1\bar{1}0]$ direction of $\text{Ag}(110)$ resulting in two possible rotational domains, as shown in Fig. 6(a). All observed two dimensional structures of H_2THPP on $\text{Ag}(110)$ are in principle related because they are based on a supramolecular arrangement very similar to the structure with an angle of the unit cell of $(70 \pm 2)^\circ$ of H_2THPP on $\text{Au}(111)$. But unlike the adsorption on $\text{Au}(111)$, the molecular assemblies on $\text{Ag}(110)$ were not continuously close-packed. One structure is characterized by periodically arranged close-packed

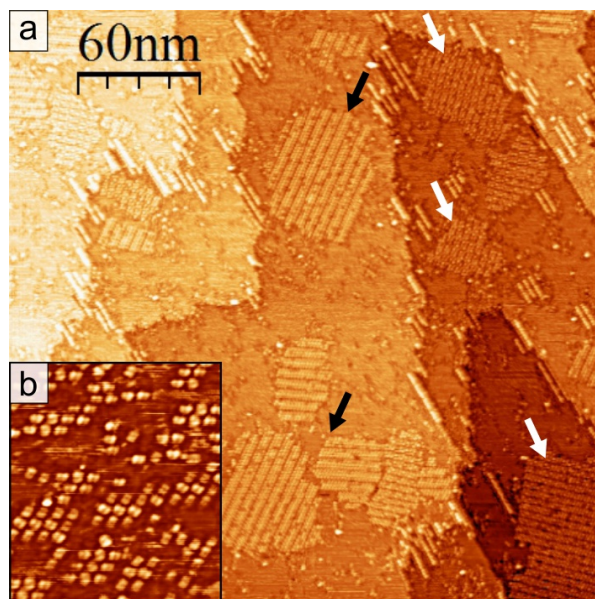


Figure 5: (a) Large scale STM image of submonolayer coverage showing molecular chains and ordered islands of H_2THPP on $\text{Ag}(110)$ (black/white arrows for the different 2D-structures, $U = 1.0$ V). (b) Aggregation into small molecular islands after the first slight annealing ($23.1 \text{ nm} \times 26.2 \text{ nm}$, $U = 1.4$ V).

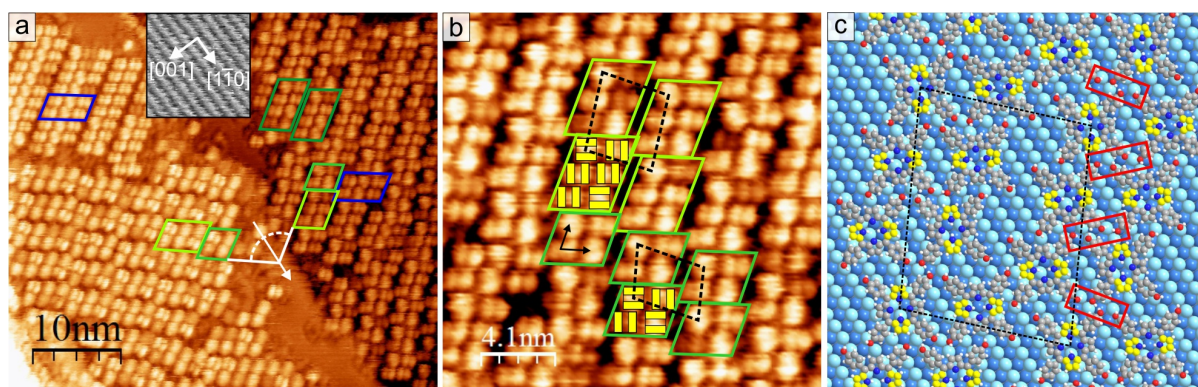


Figure 6: (a) Stripe-like structure (blue) and mirrored domains of the mixed structures consisting of close-packed blocks containing four, six or eight molecules (green rectangles); $U = 1.0$ V, $I = 100$ pA. Inset: resolved atomic rows of the $\text{Ag}(110)$ substrate ($4 \text{ nm} \times 4 \text{ nm}$, $U = 0.5$ V, $I = 1$ nA). (b) Magnification of the periodic-block structure of H_2THPP ($U = 1.0$ V). Unit cells are indicated by the black dashed parallelograms. (c) Model for the arrangement of the molecules in the structure and the epitaxy on $\text{Ag}(110)$. To emphasize the orientation, protruding carbon atoms in the macrocycle are colored yellow (yellow rectangles in (b)). First Ag layer bright blue, second layer darker blue. Sites of hydrogen bonding are marked exemplarily with red rectangles.

“blocks” containing either four ($\approx 25\%$ of island area), six (67 %) or seldom eight or more (8%) molecules (framed in green in Fig. 6). These blocks often occurred mixed because one vector of the unit cells is identical and only the length of the blocks differs. The model of this structure is shown in Fig. 6(c), where the unit cell and also the chain-wise $\text{O-H}\cdots\text{O}$ bonding between the molecules (red rectangles) is marked. The intermolecular interactions in a block increase with its size but also each shows hydrogen bonds with adjacent blocks. In total, this leads to 1.5 hydrogen bonds per molecule independent of the extent of the close-packed arrangement due to the proportionally sized unit cells. The molecules in each block have well defined, rigid orientations of the saddle-shape as marked in yellow in Fig. 6(a,c).

The second type of structure (Fig. 7) can be characterized as stripes, each with a width of three molecules. The molecular saddle-shape is rotated by 90° for molecules located diagonally

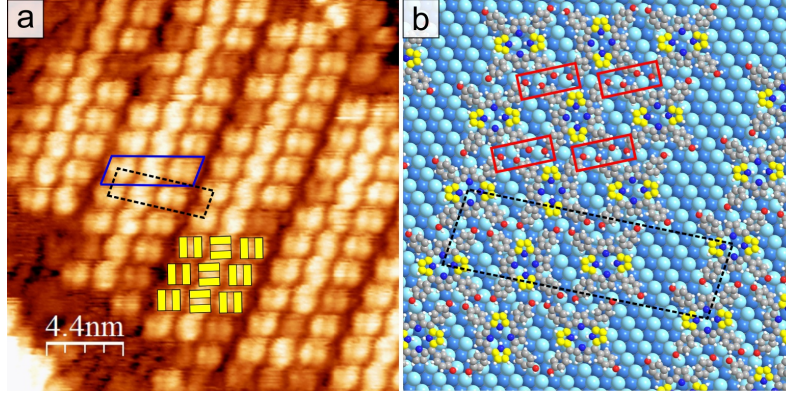


Figure 7: (a) Stripe-like structure of H_2THPP on $\text{Ag}(110)$ ($U = 1.0$ V). The unit cell (dashed parallelogram) contains an arrangement of three molecules (blue). (b) Model of epitaxy of this structure.

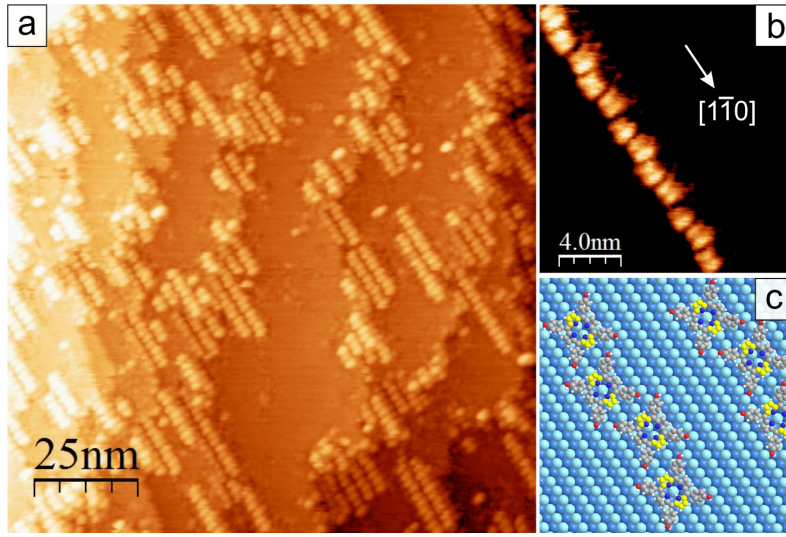


Figure 8: (a) Molecular chains along $[1\bar{1}0]$ near step edges of $\text{Ag}(110)$ ($U = 0.7$ V). (b) Magnification of a chain. H_2THPP molecules are slightly displaced in a zigzag manner ($U = 1.6$ V). (c) Model of epitaxy of the molecules in chains on $\text{Ag}(110)$.

(top left to bottom right in Fig. 7) likely again due to an interaction of the hydroxyphenyl groups, which leads to the alternating azimuthal rotation for rows of H_2THPP inside a stripe. The molecular stripe is rotated by $\approx 53^\circ$ relative to $[1\bar{1}0]$ of $\text{Ag}(110)$. Correspondingly, the molecules are rotated by $\varepsilon_1 = (30 \pm 7)^\circ$ and $\varepsilon_2 = (-60 \pm 7)^\circ$ relative to $[1\bar{1}0]$, which is also valid for H_2THPP in the blocks of the other structure. The model of the stripe-like structure is shown in Fig. 7(b), where the unit cell, which contains three molecules, is marked by a dashed rectangle. The molecular arrangement is, as previously mentioned, identical to the oblique structure on $\text{Au}(111)$. The striking difference to the periodic-block array is the continued close-packing along one direction and a width of three instead of two molecules as in the block arrangements. This leads to an increase of the intermolecular interaction with in average two hydrogen bonds per molecule. The packing density of the stripe-like structure is with (0.38 ± 0.03) molecules per nm^2 not different from those of the pattern with unit cells of four and six molecules. But they are all clearly smaller than the packing density for the previously discussed close-packed oblique structure on $\text{Au}(111)$ due to the spacing between the molecular stripes or blocks. On our samples, the stripe-like structure was the most often observed one, which indicates that it is energetically slightly more favorable than the periodic-block array.

One-dimensional chains of H_2THPP were formed along $[1\bar{1}0]$ of $\text{Ag}(110)$ as shown in Fig. 8.

These chains had, at the investigated coverage, an average length of around 12 nm. In most cases, they were located near steps of the Ag(110) surface likely because step edges are often favorable adsorption sites and starting points for further growth. The lower diffusion barrier along $[1\bar{1}0]$ compared to $[001]$ could then promote the assembly into chains. A closer look at this molecular arrangement reveals that the molecules are slightly displaced in a zigzag manner and oriented parallel to $[1\bar{1}0]$ (Fig. 8(b)). The distance between the molecules is (1.66 ± 0.05) nm and vertically between neighboring chains (3.2 ± 0.2) nm. The corresponding structural model is shown in Fig. 8(c).

The determination of the exact adsorption sites in the epitaxy of the molecular structures was inaccessible to STM imaging. However, knowledge about this is necessary to understand the influence of the Ag(110) lattice and to clarify the reason for the different supramolecular assemblies. In the following section, DFT calculations for the adsorption of H₂THPP on Au(111) and Ag(110) at different positions and rotational angles of the molecule relative to the substrate lattice will be presented and the implications for the energetic balances, responsible for the structures, be discussed.

3.3. Calculation of adsorption energies and discussion

First of all, it should be noted that for DFT the binding energy and adsorption height in general depend strongly on the approximations used. Therefore, for the investigated system several exchange-correlation functionals were tested (Fig. 9). The RPBE functional is a revised version of PBE to improve atomization and chemisorption energies for small molecules.⁴² It can be clearly seen that for physisorption like in the case of H₂THPP on Au(111), RPBE performs a lot worse than PBE due to the stronger repulsion, which leads to a shallow minimum and large underestimation of the molecule-substrate interaction. The missing non-local interaction can be compensated by adding the dispersion correction by Tkatchenko and Scheffler^{44,46} (vdW(TS)) with the van der Waals parameters for metal surfaces by Ruiz *et al.*⁴⁶ PBE+vdW(TS) gives a smaller optimal adsorption height d_{\min} compared to PBE but the adsorption energy for H₂THPP on Au(111) becomes then similar to that for the local density approximation (LDA). In general, LDA is known to overestimate binding while many xc-functionals of the generalized gradient approximation result in an underestimation. One of the topically more advanced functionals which include vdW interaction is vdW-DF2.⁵¹ This non-local correlation functional without the need of predefined dispersion coefficients gives very good adsorption energies although binding distances are still underestimated.⁴³ Our results show that when using RPBE with the vdW(TS) correction instead of PBE, the energy is now at the level of vdW-DF2 and additionally the adsorption distance is improved (Fig. 9). It should also be noted that the computational cost for RPBE+vdW(TS) is significantly lower compared to vdW-DF2. From these comparisons, we conclude that RPBE+vdW(TS) clearly gives the best description for the studied systems.

With RPBE+vdW(TS), the adsorption energy for the fully relaxed system of H₂THPP on Au(111) is -5.9 eV. The optimized geometry of H₂THPP on the surface is a saddle-shaped deformation with angles of the phenyl planes of $\phi_{\text{phenyl,ad}} = 32.5^\circ$ and pyrrole planes of $\phi_{\text{pyrrol,ad}} = 23^\circ$ relative to the surface plane. This geometry leads to the almost same adsorption height of the carbon atoms closest to the Au surface in the phenyl and the pyrrole rings. $E_{\text{ad}} - d$ curves were also calculated for the fixed geometry of H₂THPP optimized in gas-phase with $\phi_{\text{phenyl,gas}} = 65^\circ$ and $\phi_{\text{pyrrol,gas}} = 7^\circ$. Using RPBE+vdW(TS), this leads to an adsorption height higher by circa 0.15 Å and an absolute value of the adsorption energy smaller by 1.5 eV. Thus, this gain in adsorption energy justifies the ≈ 0.4 eV necessary for the deformation from a planar to a saddle-shaped macrocycle. Different adsorption sites on Au(111) and angles of azimuthal rotation relative to the substrate lattice were considered. Only a very small difference of ca. 0.05 eV is found between all of them, which indicates small energy barriers for diffusion and rotation of H₂THPP on Au(111) and, therefore, moderate mobility at room temperature (kinetic energy of

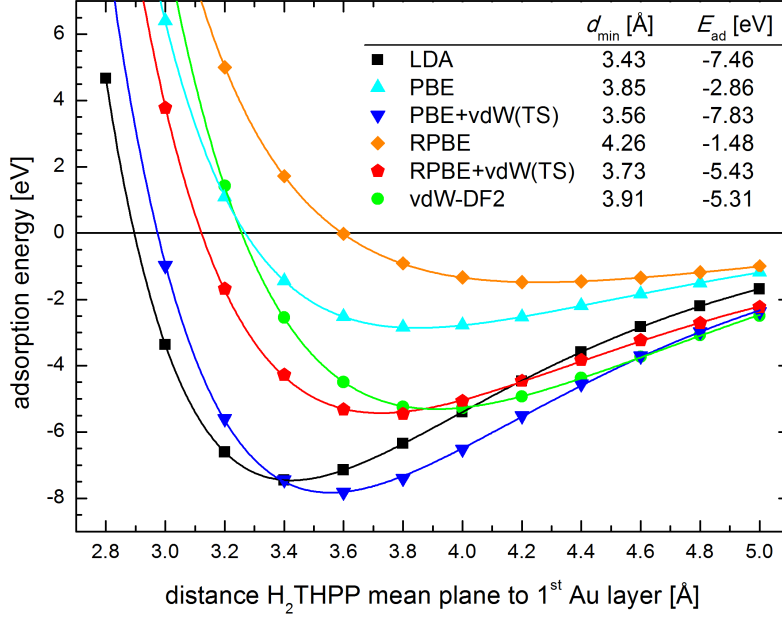


Figure 9: Adsorption energies as a function of distance d between the molecular plane of H_2THPP and the $\text{Au}(111)$ surface for different exchange-correlation functionals and dispersion corrections. The values of the energetic minima are summarized in the inserted table.

0.025 eV). A similar calculated diffusion barrier of 0.032 eV has been reported for H_2TPP on $\text{Ag}(111)$.²²

The higher corrugation of the (110) surface compared to (111) results in specific energetic favorable and unfavorable adsorption sites. Fig. 10(a) shows the model for the calculation of a single H_2THPP molecule adsorbed on $\text{Ag}(110)$ with the indicated azimuthal rotation ε of the molecule relative to $[1\bar{1}0]$. To evaluate favorable adsorption geometries, potential energy curves in dependence of ε for different adsorption sites at constant distance $d = 3.2$ Å, (average optimal adsorption height) were calculated (Fig. 10(d,e)). Compared to $\text{Au}(111)$, the adsorption of H_2THPP on $\text{Ag}(110)$ is notably stronger with higher absolute values of the adsorption energies and a smaller substrate-molecule distance, which clearly shows the known higher reactivity of the $\text{Ag}(110)$ surface. Additionally, energy barriers for molecular diffusion and rotation, which can be estimated from Fig. 10(d,e), are significantly higher than on $\text{Au}(111)$.

For H_2THPP , the intermolecular interactions determine the close-packed two dimensional structure. The molecular arrangement is then rotated relative to the substrate lattice, so that the molecules with orientations ε_1 and $\varepsilon_1 + 90^\circ$ have in total the highest absolute adsorption energy. The two angles of rotation of the molecules relative to $[1\bar{1}0]$ found by STM were $\varepsilon_1 = (30 \pm 7)^\circ$ and $\varepsilon_2 = (-60 \pm 7)^\circ$ which is identical to $+60^\circ$ due to the symmetry of the system. At both angles (marked orange in Fig. 10(d,e)), adsorption with the center in between adjacent Ag rows (position 1 and 4) led to good adsorption energies, whereas the positions on top of an Ag row (2 and 5) were the most unfavorable. Often intermediate energies were calculated for the molecular center above the slope of a Ag row (3 and 6). With this, the formation of the observed structures with gaps between the molecular blocks or stripes can now be explained. For the smallest unit (4 or 6 molecules) the interaction with the substrate is optimized through the rotation relative to $[1\bar{1}0]$. However, if the periodicity of the close-packed arrangement would be continued (as it is on $\text{Au}(111)$), some molecules would need to adsorb on the unfavorable positions on top of Ag rows, which are avoided. The model for the epitaxy of the stripe-like structure in Fig. 7(b) shows that consequently three molecules is the maximum favorable width, whereby in the unit cell one position in the middle between adjacent Ag rows and two on the slope of Ag rows are occupied by molecules. In the direction along the molecular stripe, molecules in each of the

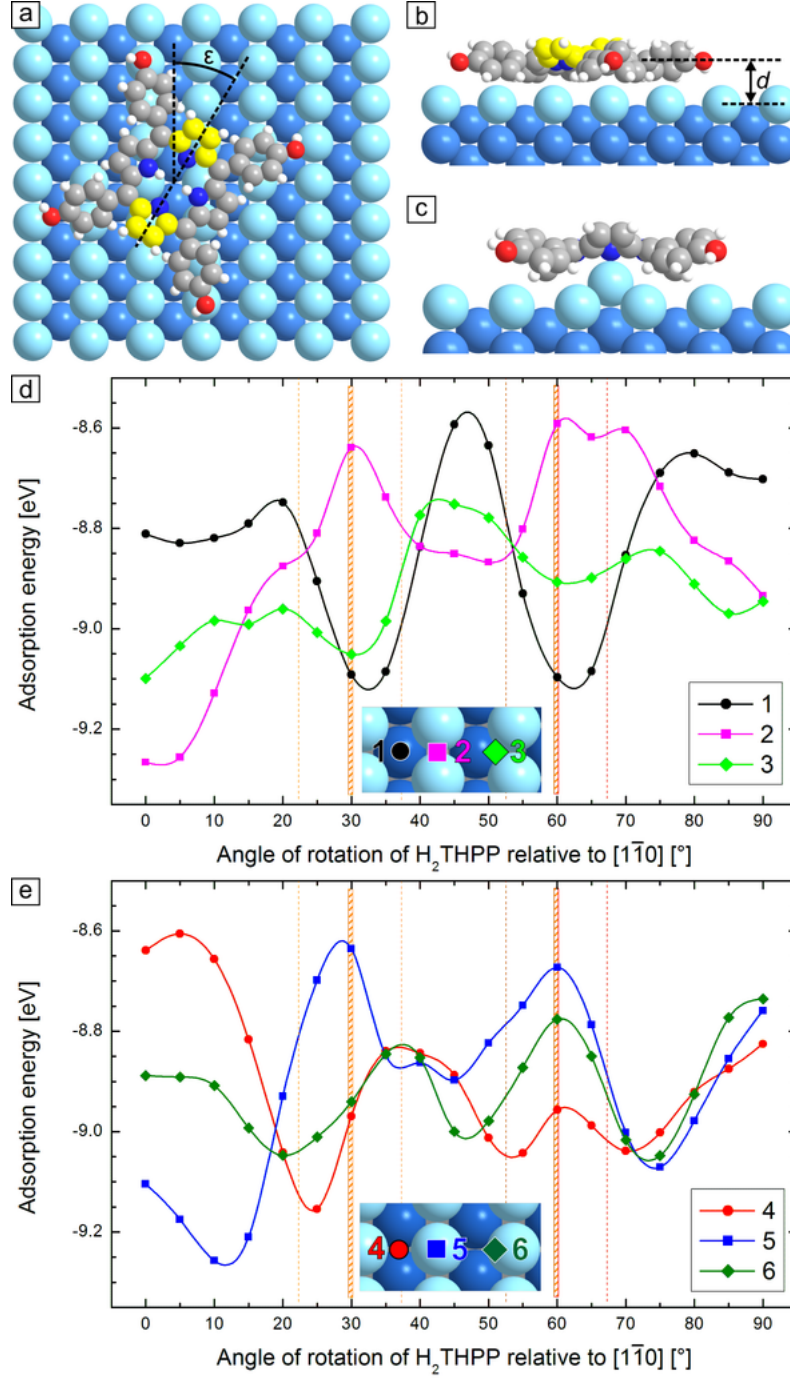


Figure 10: (a) Model of the adsorption geometry of H₂THPP on Ag(110). The angle of azimuthal rotation ε of the molecule relative to $[1\bar{1}0]$ is indicated. Investigated adsorption sites on the Ag(110) lattice are marked and numbered. The two pyrrole rings tilted away from the surface are colored yellow. (b) Side view showing the adsorption geometry at $\varepsilon = 30^\circ$ and definition of the adsorption height d . (c) Model for the adsorption on an additional protruding row of Ag adatoms. (d),(e) Adsorption energy in dependence of the azimuthal rotation of H₂THPP for the indicated adsorption positions of the molecular center at a constant height of $d = 3.2$ Å. The connecting splines are only a guide for the eye.

three rows are located on similar sites but likely incommensurately, e.g. all molecules of the central row ($\varepsilon_1 \approx 30^\circ$) with the center in between Ag rows. In the structures consisting of small molecular blocks, the discontinuation in two directions allows for the occupation of in average more energetically favorable adsorption sites. As can be seen in the model of this coincident

epitaxy in Fig. 6(b), in the unit cell with six molecules half can adsorb with the center in between Ag rows and the other half on the less favorable slope of Ag rows. However, this increased interaction with the substrate comes at the cost of less hydrogen bonds per molecule compared to the stripe-like structure, resulting in a balance.

The most favorable adsorption energies were found for $\varepsilon = 0^\circ$ or small angles of rotation relative to $[1\bar{1}0]$ and the single molecule adsorbed with the center above a silver row of the Ag(110) substrate (position 2 and 5). This matches well with H₂THPP in the molecular chains along the $[1\bar{1}0]$ direction found with STM. For the epitaxy (Fig. 8(c)), this means that the molecules are always located on the best adsorption positions. Thus, in the one-dimensional arrangement intermolecular interactions are reduced the most in favor of the best interaction with the substrate. The formations of molecular chains was also observed for a Pt-porphyrin with more bulky di-tertiary-butylphenyl-groups on Ag(110).⁵² As explanation for this linear growth behavior, the template-guided adsorption on rails of Ag adatoms was suggested. This could alternatively explain why our molecular chains of H₂THPP were mostly located near step edges because it is known that on Ag(110) at 300 K Ag atoms easily detach from step edges and are able to diffuse over the surface.^{53,54} H₂THPP molecules could then arrange over these atomic rails or capture and stabilize the Ag atoms underneath. Using DFT, the energetic minimum for the relaxed adsorption on an additional row of Ag atoms (Fig. 10(c)) was found at $E_{\text{ad}} = -9.98$ eV, which is indeed more favorable than the adsorption on the flat Ag(110) at the same molecular orientation ($\varepsilon = 0^\circ$). The small distance of 2.3 Å between the nitrogen and silver atoms indicates a strong interaction close to chemisorption. This result corroborates the suggestion of an underlying row of Ag adatoms. Nevertheless, clear experimental evidence would be needed to proof this adsorption geometry for the here studied system.

4. Conclusions

5,10,15,20-tetra(*p*-hydroxyphenyl)porphyrin molecules form highly ordered hydrogen-bonded structures in the molecular adsorbate layer. At submonolayer coverage on Au(111), the molecules self-assemble into a square arrangement characterized by pair-wise O-H...O hydrogen bonding. Near a complete monolayer, a second structure with an oblique unit cell, higher packing density and more hydrogen bonds per molecule was found. The epitaxy on Au(111) plays no major role in the supramolecular ordering. This is not the case for the adsorption on the highly anisotropic Ag(110) substrate, where the observed structures of H₂THPP are related to different balances between intermolecular interactions (number of hydrogen bonds) and the occupation of favorable adsorption positions. The strong intermolecular interactions lead to structures with an oblique molecular arrangement and well defined orientation of the saddle-shaped macrocycle similar to the adsorption on Au(111). However the short-range periodicity of the close-packed arrangement is discontinued and large unit cells are formed because unfavorable adsorption sites on the Ag(110) lattice are avoided. Furthermore, a substrate-guided growth of molecular chains of H₂THPP along the $[1\bar{1}0]$ direction of Ag(110) was found, whereby the molecule-substrate interaction is dominating.

In summary, we demonstrated the effect of strengthening intermolecular interactions between porphyrin molecules *via* hydrogen bonds, which leads to the formation of novel supra-molecular networks and complex epitaxial behaviors.

Acknowledgements

This work has been financially supported by the Deutsche Forschungsgemeinschaft (DFG) through the Research Unit FOR 1154 and the Fonds der Chemischen Industrie (FCI). Computational resources were provided by the “Chemnitzer Hochleistungs-Linux-Cluster” (CHiC) at the Technische Universität Chemnitz.

References

- [1] S. Stepanow, N. Lin, J. V. Barth, *J. Phys.: Condens. Matter* 20 (2008) 184002.
- [2] M. Hietschold, M. Lackinger, S. Griebel, W. Heckl, T. Gopakumar, G. Flynn, *Microelectron. Eng.* 82 (2005) 207.
- [3] S. Yoshimoto, N. Kobayashi, *Struct. Bond.* 135 (2010) 137.
- [4] L. Smykalla, P. Shukryna, M. Hietschold, *J. Phys. Chem. C* 116 (2012) 8008.
- [5] M. Scheffler, L. Smykalla, D. Baumann, R. Schlegel, T. Hanke, M. Toader, B. Buchner, M. Hietschold, C. Hess, *Surf. Sci.* 608 (2013) 55.
- [6] K. W. Hipps, L. Scudiero, D. E. Barlow, M. P. Cooke., *J. Am. Chem. Soc.* 124 (2002) 2126.
- [7] L. Scudiero, K. W. Hipps, D. E. Barlow, *J. Phys. Chem. B* 107 (2003) 2903.
- [8] J. P. Hill, Y. Wakayama, K. Ariga, *Phys. Chem. Chem. Phys.* 8 (2006) 5034.
- [9] C. Meier, U. Ziener, K. Landfester, P. Wehrich, *J. Phys. Chem. B* 109 (2005) 21015.
- [10] T. Gopakumar, H. Tang, W. Thiel, M. Hietschold, *J. Phys. Chem. C* 112 (2008) 7698.
- [11] M. Toader, T. G. Gopakumar, M. Abdel-Hafiez, M. Hietschold, *J. Phys. Chem. C* 114 (2010) 3537.
- [12] M. Toader, M. Knapfer, D. R. T. Zahn, M. Hietschold, *Surf. Sci.* 605 (2011) 1510.
- [13] X. Q. Tian, J. B. Xu, X. M. Wang, *J. Phys. Chem. C* 114 (2010) 20917.
- [14] G. Rojas, S. Simpson, X. Chen, D. A. Kunkel, J. Nitz, J. Xiao, P. A. Dowben, E. Zurek, A. Enders, *Phys. Chem. Chem. Phys.* 14 (2012) 4971.
- [15] T. Yokoyama, T. Kamikado, S. Yokoyama, S. Mashiko, *J. Chem. Phys.* 121 (2004) 11993.
- [16] L.-A. Fendt, M. Stohr, N. Wintjes, M. Enache, T. A. Jung, F. Diederich, *Chem. Eur. J.* 15 (2009) 11139.
- [17] D. Heim, K. Seufert, W. Auwarter, C. Aurisicchio, C. Fabbro, D. Bonifazi, J. V. Barth, *Nano Lett.* 10 (2010) 122.
- [18] J. M. Gottfried, H. Marbach, *Z. Phys. Chem.* 223 (2009) 53.
- [19] S. Yoshimoto, A. Tada, K. Suto, R. Narita, K. Itaya, *Langmuir* 19 (2003) 672.
- [20] W. Auwarter, A. Weber-Bargioni, A. Riemann, A. Schiffrin, O. Groningand, R. Fasel, J. V. Barth, *J. Chem. Phys.* 124 (2006) 194708.
- [21] W. Auwarter, K. Seufert, F. Klappenberger, J. Reichert, A. Weber-Bargioni, A. Verdini, D. Cvetko, M. Dell’Angela, L. Floreano, A. Cossaro, G. Bavdek, A. Morgante, A. P. Seitsonen, J. V. Barth, *Phys. Rev. B* 81 (2010) 245403.
- [22] G. Rojas, X. Chen, C. Bravo, J.-H. Kim, J.-S. Kim, J. Xiao, P. A. Dowben, Y. Gao, X. C. Zeng, W. Choe, A. Enders, *J. Phys. Chem. C* 114 (2010) 9408.
- [23] J. P. Beggan, S. A. Krasnikov, N. N. Sergeeva, M. O. Senge, A. A. Cafolla, *Nanotechnology* 23 (2012) 235606.
- [24] H. Wende, M. Bernien, J. Luo, C. Sorg, N. Ponpandian, J. Kurde, J. Miguel, M. Piantek, X. Xu, P. Eckhold, W. Kuch, K. Baberschke, P. M. Panchmatia, B. Sanyal, P. M. Oppeneer, O. Eriksson, *Nat. Mater.* 6 (2007) 516.
- [25] L. Smykalla, P. Shukryna, C. Mende, T. Ruffer, H. Lang, M. Hietschold, submitted to *Phys. Rev. B* (2014).
- [26] K. Ogawa, T. Zhang, K. Yoshihara, Y. Kobuke, *J. Am. Chem. Soc.* 124 (2002) 22–23.
- [27] N. A. Rakow, K. S. Suslick, *Nature* 406 (2000) 710–713.
- [28] A. J. Mozer, M. J. Griffith, G. Tsekouras, P. Wagner, G. G. Wallace, S. Mori, K. Sunahara, M. Miyashita, J. C. Earles, K. C. Gordon, L. Du, R. Katoh, A. Furube, D. L. Officer, *J. Am. Chem. Soc.* 131 (2009) 15621–15623.
- [29] S. Fukuzumi, H. Imahori, H. Yamada, M. E. El-Khouly, M. Fujitsuka, O. Ito, D. M. Guldi, *J. Am. Chem. Soc.* 123 (2001) 2571–2575.
- [30] M. Berenbaum, S. Akande, R. Bonnett, H. Kaur, S. Ioannou, R. White, U.-J. Winfield, *Br. J. Cancer* 54 (1986) 717.
- [31] R. Bonnett, R. D. White, U.-J. Winfield, M. C. Berenbaum, *Biochem. J.* 261 (1989) 277.
- [32] H. Ibrahim, A. Kasselouri, B. Raynal, R. Pansu, P. Prognon, *J. Lumin.* 131 (2011) 2528.
- [33] G. Lu, X. Zhang, X. Cai, J. Jiang, *J. Mater. Chem.* 19 (2009) 2417.
- [34] P. Bhyrappa, S. R. Wilson, K. S. Suslick, *J. Am. Chem. Soc.* 119 (1997) 8492.
- [35] S. B. Lei, C. Wang, S. X. Yin, H. N. Wang, F. Xi, H. W. Liu, B. Xu, L. J. Wan, C. L. Bai, *J. Phys. Chem. B* 105 (2001) 10838.
- [36] J. P. Hill, Y. Wakayama, M. Akada, K. Ariga, *J. Phys. Chem. C* 111 (2007) 16174.
- [37] A. Garcia-Lekue, R. Gonzalez-Moreno, S. Garcia-Gil, D. F. Pickup, L. Floreano, A. Verdini, A. Cossaro, J. A. Martın-Gago, A. Arnau, C. Rogero, *J. Phys. Chem. C* 116 (2012) 15378.
- [38] D. Hooks, T. Fritz, M. Ward, *Adv. Mater.* 13 (2001) 227.
- [39] A. D. Adler, F. R. Longo, J. D. Finarelli, J. Goldmacher, J. Assour, L. Korsakoff, *J. Org. Chem.* 32 (1967) 476.
- [40] I. Horcas, R. Fernandez, J. Gomez-Rodriguez, J. Colchero, J. Gomez-Herrero, A. Baro, *Rev. Sci. Instrum.* 78 (2007) 013705.
- [41] J. Enkovaara, C. Rostgaard, J. J. Mortensen, J. Chen, M. Dulak, L. Ferrighi, J. Gavnholt, C. Glinsvad, V. Haikola, H. A. Hansen, H. H. Kristoffersen, M. Kuisma, A. H. Larsen, L. Lehtovaara, M. Ljungberg, O. Lopez-Acevedo, P. G. Moses, J. Ojanen, T. Olsen, V. Petzold, N. A. Romero, J. Stausholm-Moller, M. Strange, G. A. Tritsarlis, M. Vanin, M. Walter, B. Hammer, H. Hakkinen, G. K. H. Madsen, R. M.

- Nieminen, J. K. Nørskov, M. Puska, T. T. Rantala, J. Schiøtz, K. S. Thygesen, K. W. Jacobsen, *J. Phys.: Condens. Matter* 22 (2010) 253202.
- [42] B. Hammer, L. B. Hansen, J. K. Nørskov, *Phys. Rev. B* 59 (1999) 7413.
 - [43] J. Klimeš, A. Michaelides, *J. Chem. Phys.* 137 (2012) 120901.
 - [44] A. Tkatchenko, M. Scheffler, *Phys. Rev. Lett.* 102 (2009) 073005.
 - [45] N. Marom, A. Tkatchenko, M. Rossi, V. V. Gobre, O. Hod, M. Scheffler, L. Kronik, *J. Chem. Theory Comput.* 7 (2011) 3944.
 - [46] V. G. Ruiz, W. Liu, E. Zojer, M. Scheffler, A. Tkatchenko, *Phys. Rev. Lett.* 108 (2012) 146103.
 - [47] A. H. Larsen, M. Vanin, J. J. Mortensen, K. S. Thygesen, K. W. Jacobsen, *Phys. Rev. B* 80 (2009) 195112.
 - [48] K. Diller, F. Klappenberger, M. Marschall, K. Hermann, A. Nefedov, C. Wöll, J. V. Barth, *J. Chem. Phys.* 136 (2012) 014705.
 - [49] M. Sinnokrot, C. Sherrill, *J. Phys. Chem. A* 108 (2004) 10200.
 - [50] J.-I. Seo, I. Kim, Y. S. Lee, *Chem. Phys. Lett.* 474 (2009) 101.
 - [51] K. Lee, Éamonn D. Murray, L. Kong, B. I. Lundqvist, D. C. Langreth, *Phys. Rev. B* 82 (2010) 081101.
 - [52] T. Yokoyama, Y. Tomita, *J. Chem. Phys.* 129 (2008) 164704.
 - [53] K. Morgenstern, E. Lægsgaard, I. Stensgaard, F. Besenbacher, *Phys. Rev. Lett.* 83 (1999) 1613.
 - [54] T. Zambelli, J. V. Barth, J. Wintterlin, *Phys. Rev. B* 58 (1998) 12663.